Quantum Mechanics in Quantum Rings

Thomas Ihn[1], Andreas Fuhrer[1], Martin Sigrist[1], Klaus Ensslin[1],
Werner Wegscheider[2], and Max Bichler[3]

[1] Solid State Physics Laboratory, ETH Zürich
    8093 Zürich, Switzerland
[2] Angew. und Exp. Physik, Universität Regensburg
    93040 Regensburg, Germany
[3] Walter Schottky Institut, TU München
    85748 Garching, Germany

Abstract. Magnetotransport measurements on a two-terminal semiconductor
quantum ring structure are reviewed. The structure has been fabricated by AFM-
lithography on a shallow Ga[Al]As heterostructure. In the open regime Aharonov-
Bohm oscillations are observed and the phase coherence length can be inferred
from their temperature dependence. The ring can also be tuned into the Coulomb
blockade regime. It is demonstrated that single-particle level spectra can be recon-
structed showing many characteristics of an ideal one-dimensional ring spectrum.
Further information about individual quantum states including their position and
degree of localisation, their angular momentum and their spin is extracted from
measurements in perpendicular and parallel magnetic field and from measurements
with asymmetrically applied plunger gate voltages. The ring is an example for a
Coulomb blockaded many-electron system in which many aspects of the energy
spectrum and the quantum states can be understood quantitatively.

1   Introduction

Within the last 100 years the implications of quantum theory have dominated
physics research. Richard Feynman states in his lectures on physics that quan-
tum interference 'has in it the heart of quantum mechanics' [1]. Within the
last fifteen years semiconductor nanostructures have proven to allow the real-
isation of nearly ideal quantum systems. Among them is the quantum point
contact showing the quantisation of conductance [2,3], quantum dots repre-
senting tunable artificial atoms [4,5] and quantum ring structures exhibiting
the Aharonov-Bohm (AB) effect [6,7,8,9]. Electron transport through these
structures at low temperatures is a key experimental technique which has
led to the discovery of a number of effects for which the phase coherence of
electrons is crucial.

   In this review we concentrate on such experiments on a nano-scale quan-
tum ring structure which gives remarkable insight into and control over quan-
tum mechanical properties of electronic states [10,11]. The review is organised
as follows: after the introduction of the structure and its fabrication we dis-
cuss the AB effect in the open two-terminal ring. When the coupling of the

ring to source and drain contacts is strongly reduced the ring can be driven into the Coulomb-blockade regime where the ring's energy spectrum and the nature of its orbital states can be investigated. In the last section we discuss how the spin states in the ring can be measured.

2   The Ring Structure and Its Fabrication

The quantum ring structure is fabricated on a Ga[Al]As heterostructure with the heterointerface 34 nm below the sample surface. The density of the two-dimensional electron gas (2DEG) forming near the interface at a temperature of $T = 4.2\,\mathrm{K}$ is $n_\mathrm{s} = 5 \times 10^{15}\,\mathrm{m}^{-2}$, its mobility is $\mu = 90\,\mathrm{m}^2/\mathrm{Vs}$.

The electron gas can be patterned into a nanostructure by local anodic oxidation [12,13]. This technique allows the direct local oxidation of a GaAs surface with the tip of a scanning force microscope under ambient conditions by applying a voltage between the conductive tip and the buried electron gas. At low temperatures the electron gas is depleted below the oxide lines. Similar to the action of a local shallow etch on the 2DEG, self-aligned but mutually insulated conducting regions are created (Fig. 1a).

Figure 1b is an image of the quantum ring structure taken after the oxidation step with the scanning force microscope. The bright lines are the oxide lines. The ring structure in the centre is connected to source and drain via quantum point contacts. These can be tuned with the in-plane gates QPC 1a and b and QPC 2a and b. Two additional plunger gates allow to tune the electronic structure of the ring. The average radius of the ring is $r_0 = 132\,\mathrm{nm}$, its electronic width about $\Delta r = 65\,\mathrm{nm}$. After the oxidation step the whole structure has been covered with a metallic top gate electrode.

Comparing the Fermi wavelength in the unstructured electron gas $\lambda_\mathrm{F} = 35\,\mathrm{nm}$ with the width of the ring Δr we estimate that 2–4 radial modes may be occupied in the ring. The elastic mean free path of electrons in the 2DEG is $l_\mathrm{e} = 8\,\mathrm{\mu m}$, much larger than the size of the whole structure.
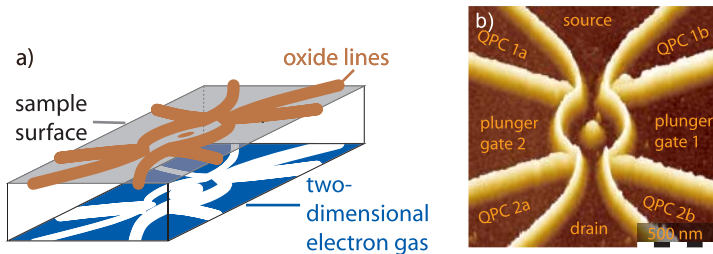

Fig. 1. (a) Schematic of the transfer of the oxide line pattern into the two-dimensional electron gas. (b) Scanning force microscopy image of the ring structure taken after writing the oxide lines but before depositing the top gate metallisation

3   Aharonov-Bohm Effect

3.1   Overview

Figure 2 shows the magnetoresistance of the ring measured at a temperature of $1.7\,\mathrm{K}$ with an AC bias current of $1.4\,\mathrm{nA}$ at $31\,\mathrm{Hz}$. The top gate voltage was $V_{\mathrm{tg}} = 300\,\mathrm{mV}$ and all in-plane gate voltages were kept at $210\,\mathrm{mV}$. These voltage settings make sure that the ring is strongly coupled to source and drain. At magnetic fields $B > 2\,\mathrm{T}$ we identify Shubnikov-de Haas minima corresponding to an electron density of $n_{\mathrm{s}} = 5.5 \times 10^{15}\,\mathrm{m}^{-2}$, e.g. close to the density in the pristine 2DEG. At low magnetic fields $B < 0.9\,\mathrm{T}$ (Aharonov-Bohm regime) pronounced B-periodic AB oscillations are observed with a period $\Delta B = 77\,\mathrm{mT}$ corresponding to a circular area with radius $131\,\mathrm{nm}$ in excellent agreement with the geometric ring radius r_0. The oscillations are strongly reduced in amplitude above $B = 0.9\,\mathrm{T}$ where the classical cyclotron radius $R_{\mathrm{c}} = \hbar k_{\mathrm{F}}/eB$ becomes smaller than r_0. At these fields the chirality of the quantum states in a magnetic field starts to play a role. Shubnikov-de Haas oscillations set in at about $2\,\mathrm{T}$ where $R_{\mathrm{c}} \approx \Delta r$. The inset shows that AB oscillations with a slightly reduced period between 65 and $70\,\mathrm{mT}$ persist even in the regime where $r_0 < R_{\mathrm{c}} < \Delta r$, but they are hardly discernible at higher fields. The reduced period reflects the increased area enclosed by the
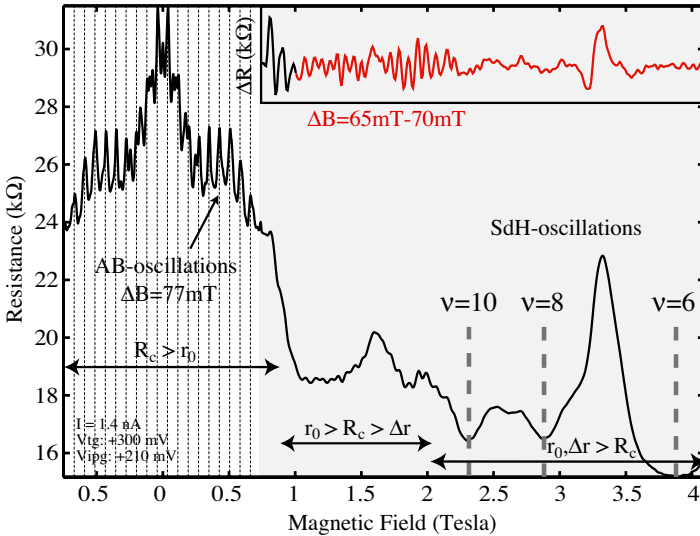

Fig. 2. Magnetoresistance of the ring measured at $T = 1.7\,\mathrm{K}$. At low magnetic fields ($B < 0.9\,\mathrm{T}$) h/e-periodic Aharonov-Bohm oscillations are visible with a period $\Delta B = 77\,\mathrm{mT}$. At large fields ($B > 2\,\mathrm{T}$) the ring shows Shubnikov-de Haas minima for even filling factors $\nu \leq 10$. The *inset* shows the magnetoresistance in this field range with the smooth background subtracted. B-periodic oscillations with slightly smaller period are observed

states as they are pushed to the outer ring boundaries by the Lorentz force. A reduction of the AB oscillation amplitude in high magnetic fields has also been observed in earlier experiments on ring structures [9,14,15].

In the remainder of this review we concentrate on measurements in the Aharonov-Bohm regime at $B < 0.9$ T where the effects of the magnetic field on the orbital wave functions play a minor role but B acts mainly on the wave function phase. In a two-terminal measurement the observable phase of the Aharonov-Bohm oscillations in the magnetoresistance is rigid due to the generalised Onsager relations [16] taking on values of either 0 or π. The magnetoresistance in Fig. 2 is symmetric around zero magnetic field in agreement with this prediction.

3.2   Phase Coherence Length from Temperature Dependence

Figure 3 shows the Aharonov-Bohm oscillations measured at three different temperatures from $T = 1.7$ K up to 15 K. At the lowest temperature the magnetoresistance shows a significant $h/2e$-periodic component. This periodicity can either arise from the interference of time reversed paths (Altshuler-Aronov-Spivak oscillations [17]) or from other paths with winding number $n = 2$ around the ring. In general, h/ne-components of the oscillations can be extracted from the measurement by Fourier analysis. The result for our measurements is shown in Fig. 4. With increasing temperature the oscillations
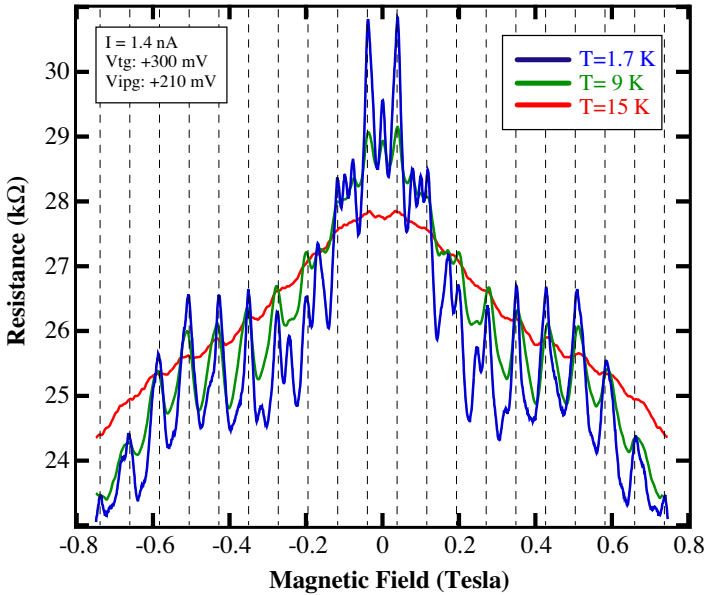

Fig. 3. Magnetoresistance of the ring measured at different temperatures. The AB oscillations decay with increasing temperature

in the magnetoresistance die out. The h/ne components disappear the faster the larger the winding number n. At $T = 15\,\mathrm{T}$ weak h/e-periodic oscillations remain.

Being an interference effect the AB oscillations require the phase coherence of electron waves. The amplitude of the oscillations is affected by dephasing [18]. The temperature dependence of the h/ne oscillation amplitude $A_n(T)$ has been suggested to follow the dependence [19]

$$A_n(T) \propto e^{-nL/l_\varphi(T)},$$

where $l_\varphi(T)$ is the temperature dependent phase coherence length and L is a characteristic length scale of the ring for which we use half the circumference, i.e. $L = \pi r_0$. It has been argued that thermal energy averaging will give a significant contribution to the temperature dependence of the h/ne-periodic oscillations for odd n as soon as kT becomes larger than the Thouless energy E_c which is in a strictly one-dimensional ring similar to the level spacing Δ [18,19]. In contrast, oscillations with even n, in particular with $n = 2$, are believed to be insensitive to thermal averaging due to the large contribution of time reversed paths [19]. The temperature dependence of these oscillations is therefore expected to be dominated by $l_\varphi(T)$. From these arguments a temperature dependence $l_\varphi(T) \propto T^{-1}$ was found in recent experiments in a temperature range between 0.3 and 3.5 K [19], similar to the behaviour in small open dots [20].

In our experiment the temperature dependence of the $h/2e$-periodic oscillations does not strictly follow the $1/T$-dependence over the full temperature range (Fig. 4). Other dephasing mechanisms in addition to electron-electron scattering may lead to a stronger decay at higher temperatures. If we estimate the phase coherence length from the data points below 6 K assuming the $1/T$-dependence to hold, we find $l_\varphi(T) = 7.5\,\mu\mathrm{m}/(T/\mathrm{K})$. In addition, we find that the decay of h/ne-periodic oscillations is proportional to n for $n \leq 3$,
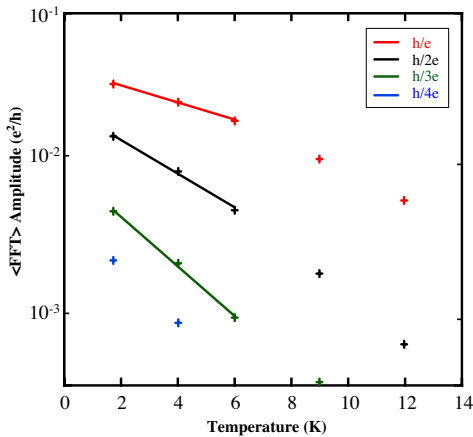

Fig. 4. Amplitudes of h/ne-periodic oscillations determined from a Fourier-analysis of the magnetoconductances at different temperatures

i.e. thermal energy averaging does not seem to dominate in our structure for odd n. This result which is in contrast to previous experiments [19] may be due the more than a factor of ten larger level spacing $\Delta \propto 1/r_0^2$ caused by our small ring radius r_0.

4   The Ring in the Coulomb-Blockade Regime

For the following experiments the ring was cooled down to $100\,\mathrm{mK}$ in a dilution refrigerator. A DC bias voltage of $V_{\mathrm{bias}} = 20\,\mu\mathrm{V}$ was applied between source and drain contacts and the DC current was measured with a noise floor at about $200\,\mathrm{fA}$.

The quantum ring structure can be tuned into the Coulomb blockade regime [10,11] by lowering the top gate voltage to $V_{\mathrm{tg}} \approx 210\,\mathrm{mV}$ and setting the voltages of the point contact gates $V_{\mathrm{QPC1a}} = V_{\mathrm{QPC1b}} = 200\,\mathrm{mV}$ and $V_{\mathrm{QPC2a}} = V_{\mathrm{QPC2b}} = 300\,\mathrm{mV}$. Plunger gate voltages were kept between 200 and $300\,\mathrm{mV}$.

4.1   Coulomb Blockade Diamonds

The differential conductance dI/dV_{bias} is shown in Fig. 5 as a function of V_{bias} and V_{tg}. Along the dashed line of zero bias conductance resonances can be seen at discrete V_{tg}. The diamond shaped regions of small differential conductance lining up along the same axis are Coulomb blockade diamonds characteristic for regions of fixed electron number in the ring [21,22]. From one diamond to the next the number of electrons increases by one with increasing V_{tg}. Half the width of a certain diamond in V_{bias}-direction gives the energy (divided by the electronic charge e) for adding the next electron to the dot. In the constant interaction picture [23] it is given by the sum of the charging energy contribution e^2/C_Σ and the single-particle level spacing Δ_i. For the diamond marked by white boundary lines in Fig. 5 this energy is $300\,\mu\mathrm{eV}$. The separation of conductance peaks at zero bias is given by the same energy allowing to determine the lever arm of the top gate to be $\alpha_{\mathrm{tg}} = 0.6$. This lever arm is constant over the whole voltage range shown in the figure. It allows the conversion of V_{tg} into an energy scale which is important for a quantitative spectroscopy of states in the ring.

4.2   Voltage Dependent Lever Arms

In contrast to α_{tg} the lever arms of the in-plane plunger gates α_{pg} are not constant. This is shown in Fig. 6a where the DC conductance is plotted for constant $V_{\mathrm{bias}} = 20\,\mu\mathrm{V}$ and variable top gate and plunger gate voltages (the plunger gate voltage is applied to both plunger gates in Fig. 1b). The reason for the voltage dependent α_{pg} is the finite density of states in the two-dimensional in-plane gates, which leads to substantial depletion of these gates
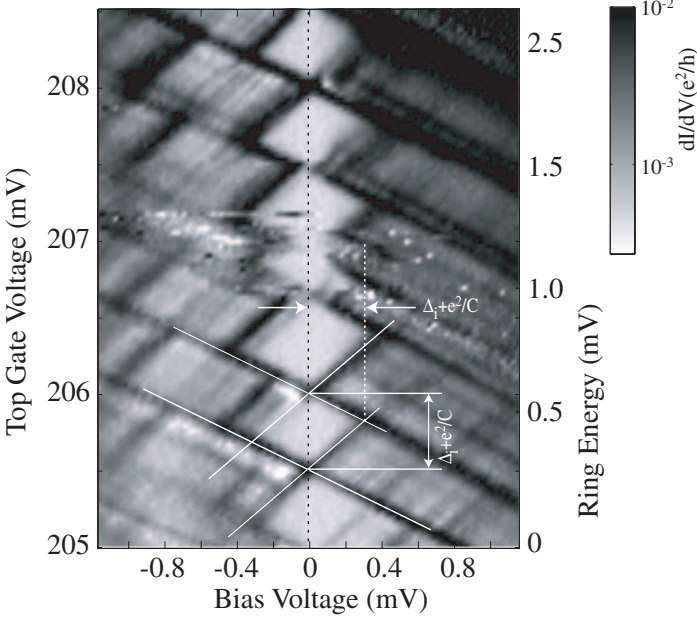
Fig. 5. The differential conductance dI/dV_{bias} as a function of top gate and bias voltage shows Coulomb blockade diamonds. The plunger gate voltage was $V_{\mathrm{pg}} = 300\,\mathrm{mV}$

near the ring at negative $V_{\mathrm{tg}} - V_{\mathrm{pg}}$. The dashed lines in the figure indicate parametric charge rearrangements in the sample. Given that α_{tg} is independent of the gate voltages, the V_{tg} axis in Fig. 6a can be directly converted to an energy scale. We further observe that on lines of constant $V_{\mathrm{tg}} - V_{\mathrm{pg}}$ (these lines are essentially parallel to the V_{tg}-axis, i.e. at constant V_{pg}) different conductance peaks have with good accuracy the same slope $dV_{\mathrm{tg}}/dV_{\mathrm{pg}}$. We determine the voltage dependent differential lever arm

$$\alpha_{\mathrm{pg}}(V_{\mathrm{pg}}) = \alpha_{\mathrm{tg}} \frac{d(eV_{\mathrm{tg}})}{dV_{\mathrm{pg}}}$$

by averaging the slopes for different peaks at given V_{pg}. Integration of the differential lever arm gives the desired energy calibration for the V_{pg}-axis. Figure 6b shows the success of the procedure by plotting the peaks of Fig. 6a with two renormalised energy axes. All peaks have a slope of -1 by construction. The same calibration procedure can be performed for each plunger gate individually. It turns out that the corresponding differential lever arms $\alpha_{\mathrm{pg}i}(V_{\mathrm{pg}i})$ are identical for both plunger gates ($i = 1, 2$) demonstrating their symmetric action on the states in the ring. Figs. 6c and d show the convincing results.
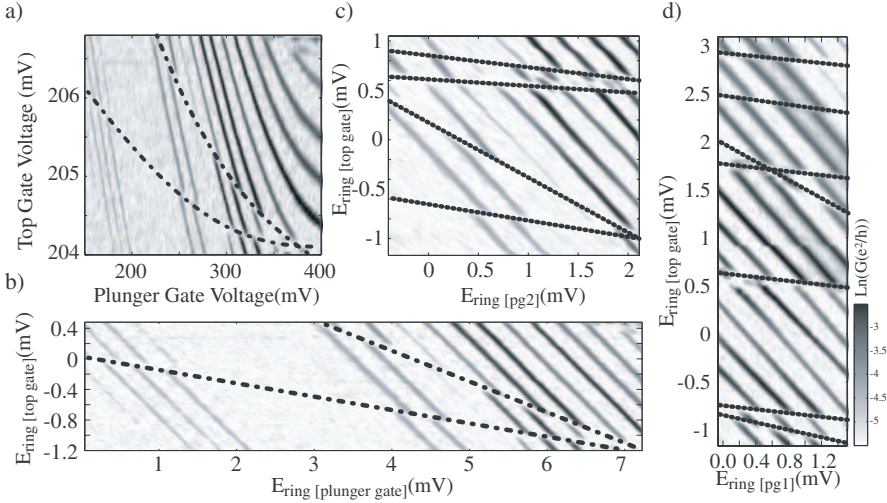
Fig. 6. (a) The conductance G as a function of top gate and plunger gate voltage shows the voltage dependent lever arm of the plunger gate. (b) After converting the V_{pg} and the V_{tg}-axis to an energy scale all conductance peaks move along lines with slope of -1. (c) and (d) The same calibration works for the two individual plunger gates

4.3   Energy Spectra as a Function of Magnetic Field

The electron in a one-dimensional ring pierced by a magnetic flux (Fig. 7a) has become a popular analytically solvable model in quantum mechanics courses. The Schrödinger equation can be written in the form [24]

$$\left[\frac{1}{2m^\star}\left(\hat{p}+\hbar k\right)^2+V(x)\right]u_k(x)=E_k u_k(x), \tag{1}$$

where $k=\Phi/(r_0\Phi_0)=\pi r_0 eB/h$ is the renormalised magnetic field, the co-ordinate x is measured along the ring circumference and $\hat{p}=-i\hbar\partial/\partial x$ is the momentum operator. An arbitrary potential $V(x)$ is allowed around the ring, which has the property $V(x+2\pi r_0 n)=V(x)$ for an arbitrary integer n. The wave function $u_k(x)$ is also required to be periodic around the ring. Using the Ansatz for a Bloch wave $\psi_k(x)=u_k(x)\exp(ikx)$ one can show that the $\psi_k(x)$ obey the equation

$$\left[\frac{\hat{p}^2}{2m^\star}+V(x)\right]\psi_k(x)=E_k\psi_k(x),$$

which describes the problem of an electron in a one-dimensional periodic potential $V(x)$. The eigenvalue solutions of this problem are, of course, well known (see e.g. [25,24]) and we show them schematically in Fig. 7b and c. If the potential $V(x)$ which breaks the rotational symmetry of the problem is
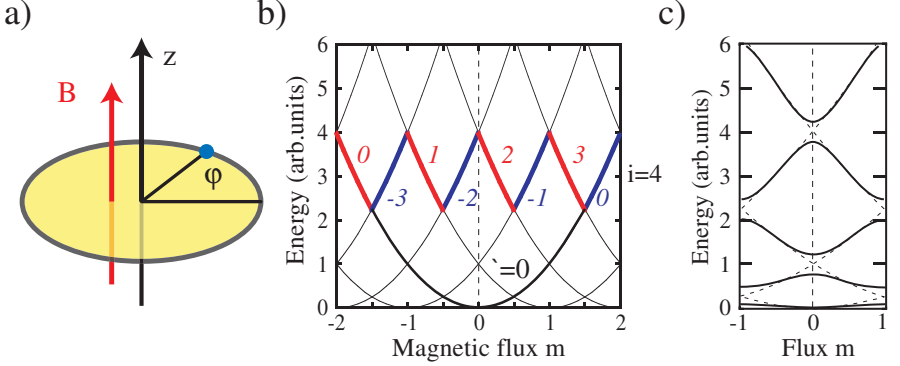
a)   b)   c)

Fig. 7. (**a**) Schematic of the one-dimensional ring problem. (**b**) Energy spectrum for $V(x) = 0$. The flux piercing the ring is measured in dimensionless units $m = \Phi/\Phi_0$, where $\Phi_0 = h/e$ is the flux quantum. Numbers along the zig-zag line are the angular momenta of the corresponding states. (**c**) Energy spectrum for $V(x) = 0$ (*dashed parabolae*) and $V(x) \neq 0$ (*solid lines*) in the reduced zone scheme

zero, we have the free-electron case and the spectrum consists of parabolae shifted with respect to each other by one flux quantum. Characteristic for the resulting energy spectrum in Fig. 7b are the diamond shaped regions enclosed by energy states. Alternatively the one-dimensional ring states can be described in terms of the angular momentum quantum number ℓ [10]. Each parabola in Fig. 7b corresponds to a certain angular momentum such that $\ell = m$ at the apex of the parabola, where $m = \Phi/\Phi_0$ is the number of flux quanta threading the ring, i.e.

$$E_\ell(m) = \frac{\hbar^2}{2m^\star r_0^2}(\ell - m)^2. \tag{2}$$

In case of non-zero $V(x)$ (weak periodic potential) the dispersion splits at degeneracy points and forms a 'band structure' (Fig. 7c). Filling such a ring spectrum with a constant electron number, we observe that the topmost state changes its energy in a zig-zag fashion as a function of magnetic flux (Fig. 7b and c). Introducing interactions in the spirit of the constant inter-action model, neighboring 'bands' in Fig. 7c will additionally split by the charging energy e^2/C_Σ and each individual 'band' will split into a spin-pair with the same spacing.

Figure 8a shows the measured conductance of the ring as a function of plunger gate voltage and magnetic field taken at $V_{tg} = 213\,\mathrm{mV}$, i.e. at a different top gate voltage than the corresponding measurement in [10]. The dispersions of the conductance peaks in a magnetic field show the Aharonov-Bohm period of $\Delta B = 75\,\mathrm{mT}$ in peak position as well as in amplitude, about the same value found for the oscillating conductance in the open regime (Fig. 2). Under the reasonable assumption of a magnetic field independent
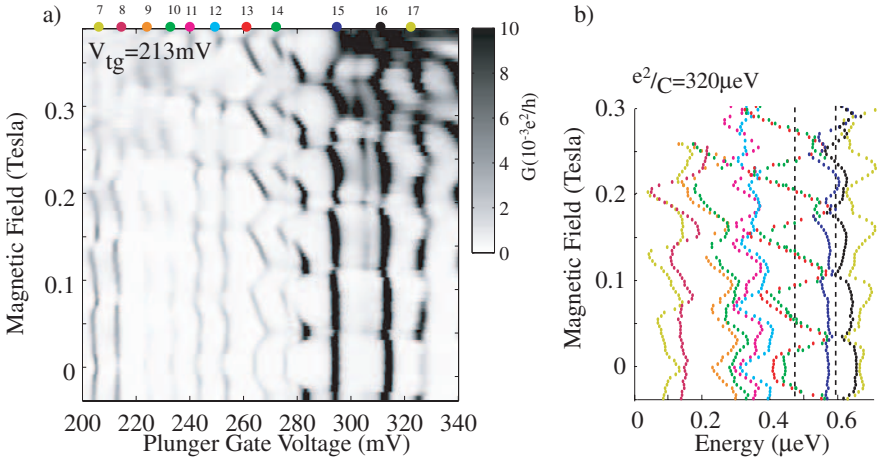
Fig. 8. (**a**) Measured conductance as a function of plunger gate voltage and magnetic field. (**b**) Reconstructed energy spectrum. A constant charging energy of 320 μV was subtracted between neighbouring conductance peaks

charging energy the motion of the peaks as a function of magnetic field does directly reflect the dispersion of single-particle states. Pronounced zig-zag behaviour as expected from the one-dimensional model is, for example, seen for the peaks labeled 13 and 14. Obviously these two peaks are a spin-pair, i.e. they belong to the same orbital level successively populated by spin-up and down with increasing V_{pg}. No significant rounding of the cusps along these lines is observed indicating that the symmetry breaking potential felt by these states is small. Other conductance peaks do not show such a pronounced zig-zag behaviour but have a weaker magnetic field dispersion. They look rather like the lowest states in Fig. 7c which are strongly influenced by the potential $V(x)$. Considering that two or more radial subbands coexist in the ring structure we have to expect the superposition of two or more 'band structures' like the one in Fig. 7c offset by the subband splitting with respect to each other. Such a scenario leads to many accidental level crossings reducing the probability for the occurrence of strongly oscillating states. At the same time this consideration explains the coexistence of flat as well as strongly oscillating states which are close in energy.

It has been demonstrated in [10] that an experimental single-particle energy spectrum can be reconstructed from measurements like Fig. 8a if a constant charging energy is subtracted between conductance peaks. The result of this procedure is shown in Fig. 8b. Already in this figure, the presence of diamonds characteristic for the ideal one-dimensional ring spectrum (Fig. 7b) can be seen. In Fig. 9 measurements taken at three slightly different top gate voltages have been combined in order to reconstruct a spectrum with as many states as possible. In this spectrum, many diamonds like the shaded one are
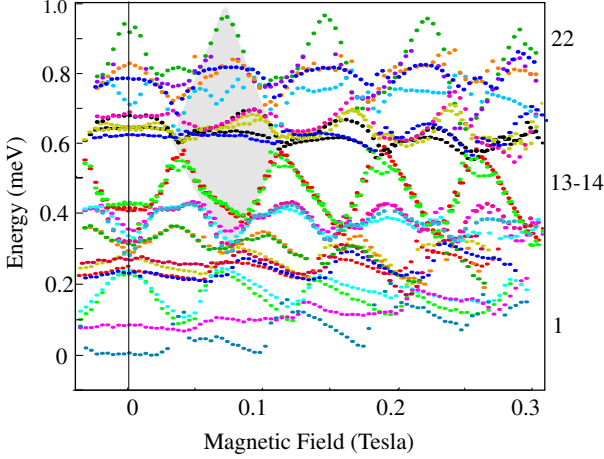
Fig. 9. Reconstructed energy spectrum. Conductance peak positions were shifted by appropriate values close to the charging energy, in contrast to Fig. 8b, where a constant charging energy was used for reconstructing the spectrum

discernible reminding of the one-dimensional model. Even the parabolic dispersions of states with given angular momentum can be followed over a large energy interval. The additional states with a weaker dispersion are due to low lying states of another subband.

An upper limit for the electron number N in the ring can be estimated from the product of the electron density n_s in the 2DEG and the ring area $A = \pi(r_0 + \Delta r/2)^2 - \pi(r_0 - \Delta r/2)^2$ giving $N < 270$. A lower limit for N can be obtained as follows: from the slope of the strongly oscillating zig-zag states such as 13 and 14 and using eq. (2) we can determine the associated angular momentum ℓ at $B = 0$ to be about 8. This implies that there are 17 spin degenerate angular momentum states occupied in this subband accommodating 34 electrons. Additional electrons will fill states of at least one additional subband. Just counting the corresponding conductance peaks at $B = 0$ in Fig. 9 gives ten additional electrons. We are confident that the actual electron number is $N > 50$. From these estimates it becomes evident that the ring is a many-electron quantum dot. In the literature, energy spectra of few-electron quantum dots have been analysed in detail and shell-filling has been found in so-called artificial atoms [4]. Energy spectra of many-electron quantum dots have so far been analysed by statistical approaches such as random matrix theory (see [26,27] for excellent reviews).

The quantum ring structure discussed here is an example for a many-electron quantum dot in which many aspects of the energy spectrum and the quantum states can be understood quantitatively and many others at least qualitatively.

We support this central statement by a few examples some of which have been discussed in other publications [10,11]. As shown above, angular momentum quantum numbers can be determined from the slopes of the strongly oscillating zig-zag states. This implies that the corresponding wave functions are close to plane wave states extended around the ring. As discussed in [11] the contribution of these states to the persistent currents in the ring is significant and can be quantitatively determined from the spectrum. On the other hand, states with a weak magnetic field dispersion will tend to be localised by some symmetry breaking potential $V(x)$. The wave functions are, however, of such a shape that the states still couple sufficiently to source and drain and a conductance resonance is detected. Localisation of states may therefore most likely occur in the vicinity of source and drain, or in one of the two arms of the ring. We will come back to this issue further below. It has also been shown [11] that interaction effects can be explained quantitatively based on a Hartree-calculation. Screening of the interaction by the presence of the top gate lowers the charging energy significantly. For the same reason the typical exchange energy is negligibly small. Under the assumption of negligible fluctuations of the charging energy this explains why spin-pairs occur in this sample with exceptionally high frequency.

4.4   Asymmetric Plunger Gate Voltages

The nature of states in the ring being either extended (strong dispersion in B, well defined ℓ) or localised (flat dispersion in B) can be further investigated by the application of asymmetric plunger gate voltages. The basic idea is that states localised in the arm near plunger gate 1 will strongly shift in energy when this plunger gate is changed, but weakly shift if plunger gate 2 is changed due to the different lever arms of the two gates on such a state. A state which is symmetric with respect to the axis connecting source and drain is in first order not shifted at all when $V_{pg1} - V_{pg2}$ is changed while $(V_{pg1} + V_{pg2})/2$ is kept fixed.

Figure 10a shows the dispersion of three neighbouring states measured at $B = 2\,\mathrm{mT}$ as a function of the asymmetry parameter α given by the difference $V_{pg1} - V_{pg2}$ converted to energy using the voltage dependent lever arms discussed before. The average voltage $(V_{pg1} + V_{pg2})/2$ converted to energy serves as the energy parameter δ. A constant charging energy of $310\,\mu\mathrm{eV}$ has been subtracted from the separation of neighbouring peaks. Around zero asymmetry, states 1 and 2 move strongly to higher energy with increasing α while state 3 depends weakly on asymmetry. We conlude that states 1 and 2 are more localised close to plunger gate 2, but state 3 is extended around the ring. Comparison with the magnetic field dispersion of these three states shown in Fig. 10b strongly supports this conlusion. Around zero magnetic field states 1 and 2 are constant in energy, i.e. localised, state 3 has a large slope, i.e. it has a well defined angular momentum and extends evenly around
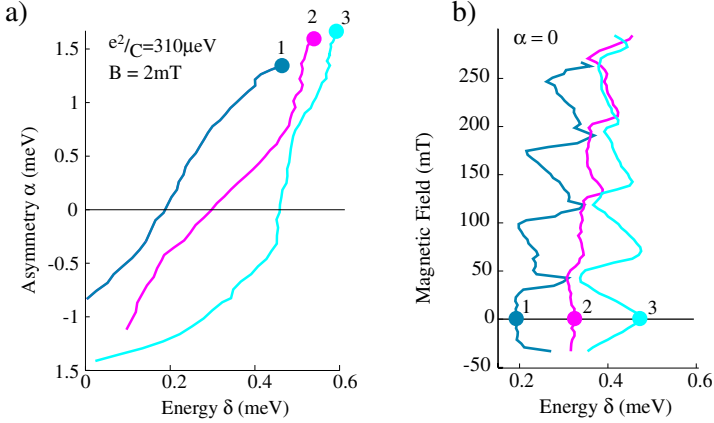
a)

Fig. 10. (**a**) Dispersion of three neighbouring quantum states as a function of asymmetrically applied plunger gate voltages. Conductance peak positions were shifted by 310 μeV. (**b**) The dispersion of the same conductance peaks as a function of magnetic field

the ring. This example shows how the combination of conductance measurements at zero asymmetry but in a magnetic field and those at zero magnetic field and finite asymmetry gives further insight in the nature of the observed quantum states of the Coulomb-blockaded many-electron quantum ring system. A careful analysis of a larger number of states confirms the interpretation developed above.

4.5   Zeeman Splitting of Spin-Pairs in Parallel Magnetic Field

In the preceeding discussion of experimental spectra neighbouring zig-zag states have been interpreted as spin-pairs. It is possible to access the spin of the tunnelling electron directly by applying the magnetic field parallel to the plane of the ring [28]. In Fig. 11a we show two conductance peaks corresponding to a spin-pair measured as a function of perpendicular magnetic field. After this measurement the sample was rotated in situ into the parallel magnetic field orientation (with very high accuracy) keeping the temperature below 600 mK. After the rotation was finished the peak separation was unchanged for all the measured conductance peaks (most of them are not shown here). Figure 11b shows the peaks corresponding to the spin-pair as a function of parallel magnetic field. The separation of the peaks increases linearly with $B_{\parallel}$ as expected for Zeeman splitting of spin-up and spin-down. This proves directly that the interpretation of the two zig-zag states observed in $B_{\perp}$ as a spin-pair is correct.

The diamagnetic shift of levels in $B_{\parallel}$ which plays an important role in [28] is relatively weak in the quantum ring. It leads to a slight shift of both peaks to higher energies as $B_{\parallel}$ increases. This shift is the same for the two
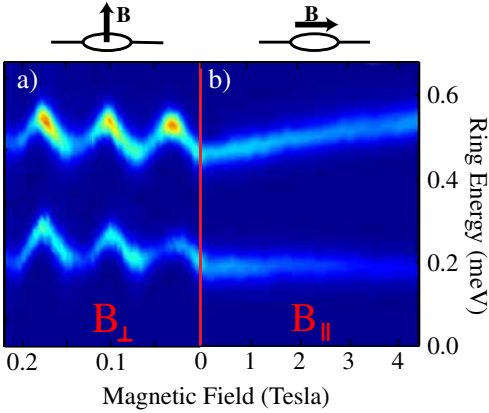
Fig. 11. (**a**) Conductance peaks of a spin-pair measured in perpendicular magnetic field. (**b**) The same conductance peaks after in situ rotation of the ring into the parallel magnetic field orientation measured as a function of parallel field. The change in peak separation is the Zeeman splitting of spin-up and down electrons

peaks because the corresponding orbital wave functions of the two states are identical.

5   Outlook

This review has tried to give an overview over recent magnetotransport experiments on a quantum ring sample fabricated by AFM-lithography. Some results like the Aharonov-Bohm oscillations and the dephasing in the open ring, the measurements in the Coulomb blockade regime with asymmetric plunger gate voltages and the Zeeman splitting have not been published before. Similar reconstructed energy spectra as a function of $B_\perp$ and questions related to the screened interactions and persistent currents have been discussed in [10,11]. All the interpretation of the spectra presented here used the constant interaction picture.

However, a close inspection of the data reveals effects beyond this simple model. Variations of the charging energy around an average value can be related to the extended or localised character of the states. Under very special circumstances, even the exchange energy shows up and one can speculate about the existence of voltage tunable singlet-triplet transitions. Such transitions can also be observed at finite $B_\parallel$. From the observation of Zeeman shifts of a larger number of peaks one can try to infer information about the ground state spin of the quantum ring similar to [28]. The Kondo-effect has been observed in this ring when the coupling to source and drain was increased. Its strength can be shown to vary with magnetic field in a h/e-periodic fashion. All these results will be discussed in detail in future publications.

Quantum rings are also interesting from different viewpoints. Being the standard interferometers in mesoscopic semiconductor physics they have, for example, been used for the measurement of the transmission phase through a quantum dot embedded in one arm of a ring [29,30]. The detailed understanding of these experiments, in particular the observed phase lapse between conductance peaks, is still controversial and further experiments are certainly needed. Recent experiments on rings with a quantum dot embedded in both arms showed signatures of the Fano effect [31]. In connection with experiments aiming at controlled dephasing [32] high quality quantum rings that can be coupled to other quantum devices are highly desirable. Given the present interest in phase coherence, dephasing, entanglement and interactions in view of quantum information processing, one can certainly state that experiments with quantum rings promise still many exciting results in the future.

References

1. R. Feynman, R. Leighton, and M. Sands, *The Feynman Lectures on Physics, Vol. III* (Addison Wesley, 1965). 139

2. B. van Wees, H. van Houten, C. Beenakker, J. Williamson, L. Kouwenhoven, D. van der Marel, and C. Foxon, Phys. Rev. Lett. **60**, 848 (1988). 139

3. D. Wharam, T. Thornton, R. Newbury, M. Pepper, H. Ahmed, J. Frost, D. Hasko, D. Peacock, D. Ritchie, and G. Jones, J. Phys. C **21**, L209 (1988). 139

4. S. Tarucha, D. Austing, T. Honda, R. van der Haage, and L. Kouwenhoven, Phys. Rev. Lett. **77**, 3613 (1996). 139, 149

5. L. Kouwenhoven, D. Austing, and S. Tarucha, Rep. Prog. Phys. **64**, 701 (2001). 139

6. G. Timp, A. Chang, J. Cunningham, T. Chang, P. Mankiewich, R. Behringer, and R. Howard, Phys. Rev. Lett. **58**, 2814 (1987). 139

7. K. Ishibashi, Y. Takagaki, K. Gamo, S. Namba, S. Ishida, K. Murase, Y. Aoyagi, and M. Kawabe, Solid State Communications **64**, 573 (1987). 139

8. C. Ford and H. Ahmed, Microelectronic Engineering **6**, 169 (1987). 139

9. G. Timp, A. Chang, P. DeVegvar, R. Howard, R. Behringer, J. Cunningham, and P. Mankiewich, Suf. Sci. **196**, 68 (1988). 139, 142

10. A. Fuhrer, S. Lüscher, T. Ihn, T. Heinzel, K. Ensslin, W. Wegscheider, and M. Bichler, Nature **413**, 822 (2001). 139, 144, 147, 148, 150, 152

11. T. Ihn, A. Fuhrer, T. Heinzel, K. Ensslin, W. Wegscheider, and M. Bichler, Physica E **16**, 83 (2003). 139, 144, 150, 152

12. R. Held, T. Vancura, T. Heinzel, K. Ensslin, M. Holland, and W. Wegscheider, Appl. Phys. Lett. **73**, 262 (1998). 140

13. T. Heinzel, R. Held, S. Lüscher, K. Ensslin, W. Wegscheider, and M. Bichler, Physica E **9**, 84 (2001). 140

14. G. Timp, P. Mankievich, P. deVegvar, R. Behringer, J. Cunningham, R. Howard, H. Baranger, and J. Jain, Phys. Rev. B **39**, 6227 (1989). 142

15. J. Liu, W. Gao, K. Ismail, K. Lee, J. Hong, and S. Washburn, Phys. Rev. B **50**, 17383 (1994). 142

16. M. Büttiker, Phys. Rev. Lett. **57**, 1761 (1986).   142
17. B. Altshuler, A. Aronov, and B. Spivak, JETP Lett. **33**, 94 (1981).   142
18. Y. Imry, *Introduction to Mesoscopic Physics*, vol. 1 of *Mesoscopic Physics and Nanotechnology* (Oxford University Press, 2002), 2nd ed.   143
19. A. E. Hansen, A. Kristensen, S. Pedersen, C. B. S. rensen, and P. E. Lindelof, Phys. Rev. B **64**, 45327 (2001).   143, 144
20. A. Huibers, M. Switkes, C. Marcus, K. Campman, and A. Gossard, Phys. Rev. Lett. **81**, 200 (1998).   143
21. E. Foxman, P. McEuen, U. Meirav, N. Wingreen, Y. Meir, P. Belk, N. Belk, M. Kastner, and S. Wind, Phys. Rev. B **47**, 10020 (1993).   144
22. L. Kouwenhoven, C. Marcus, P. McEuen, S. Tarucha, R. Westervelt, and N. Wingreen, in *Nato ASI conference proceedings*, edited by L. P. Kouwenhoven, G. Schön, and L. Sohn (Kluwer, Dordrecht, 1997), pp. 105–214.   144
23. C. Beenakker, Phys. Rev. B **44**, 1646 (1991).   144
24. M. Büttiker, Y. Imry, and R. Landauer, Phys. Lett. **96A**, 365 (1983).   146
25. N. W. Ashcroft and N. D. Mermin, *Solid State Physics* (Saunders College Publishing, 1976).   146
26. C. Beenakker, Rev. Mod. Phys. **69**, 731 (1997).   149
27. Y. Alhassid, Rev. Mod. Phys. **72**, 895 (2000).   149
28. S. Lindemann, T. Ihn, T. Heinzel, W. Zwerger, K. Ensslin, K. Maranowski, and A. Gossard, Phys. Rev. B **66**, 195314 (2002).   151, 152
29. A. Yacoby, M. Heiblum, D. Mahalu, and H. Shtrikman, Phys. Rev. Lett. **74**, 4047 (1995).   153
30. R. Schuster, E. Buks, M. Heiblum, D. Mahalu, V. Umansky, and H. Shtrikman, Nature **385**, 417 (1997).   153
31. K.Kobayashi, H.Aikawa, S.Katsumoto, and Y.Iye, Phys.Rev.Lett **88**, 256806 (2002).   153
32. E. Buks, R. Schuster, M. Heiblum, D. Mahalu, and V. Umansky, Nature **391**, 871 (1998).   153